Advances and Applications in Fluid Mechanics

Published Online: October 2016
http://dx.doi.org/10.17654/FM019040837
Volume 19, Number 4, 2016, Pages 837-849 **ISSN: 0973-4686**

AERODYNAMIC PERFORMANCE EVALUATION OF HUMPBACK WHALE INSPIRED WIND TURBINE BLADE USING CFD

P. Viswanathan, T. Prabu, S. Sivasubramaniam and R. Rudramoorthy

Department of Mechanical Engineering
PSG College of Technology
Coimbatore 641014, India

Abstract

As the need for energy is rising, the generation capacity has to be improved. While increasing the generation capacity, it is very important that the generation methods do not spoil the environment. Wind energy is a clean green and a renewable energy source, which was available in much concentrated form. The wind turbines which convert the available wind into useful power require a very high wind speed in the range from 11m/s to 25m/s. The horizontal axis wind turbines are not effective in the low wind regimes and urban environment. The shape of the airfoil for the wind turbines is adopted from of the standard NACA profiles. The aerodynamic performance of these airfoils is not efficient. In this work, the section of the blade was mimicked from the fins of the hump back whale and analyzed for the aerodynamic performance characters such coefficient of lift (C_L) and coefficient of drag (C_d) using CFD Fluent software. A comparative analysis was made between a standard NACA 0012 blade section and

Received: June 8, 2016; Accepted: October 2, 2016
2010 Mathematics Subject Classification: 76-04.
Keywords and phrases: humpback whales, coefficient of lift, coefficient of drag, bumped leading edge, airfoil for low wind regime.
Communicated by Shahrdad G. Sajjadi

a mimicked bumped edged NACA 0012 blade section. The angle of attack (AOA) was able be to increased upto 25° without of much stall and the increase in lift coefficient was 24%. Thus, these results of this work had created interest in modifying the blade profiles for the wind turbine operating in low wind regimes and urban environment.

1. Introduction

As the availability of the fossil fuels is getting depleted and the need for sustainable growth of science increases, the production of power from the renewable energy sources gains momentum [1]. The wind energy is one, which is renewable, clean, green and does not impact on the environment. According to Albert Betz, the maximum possible conversion factor from wind is only 59.3% [2]. The researchers were working in order to increase the time period of power production by operating the wind turbines at low velocity and reducing the stall caused due to the boundary layer separation over the aerofoil structure. In order to prevent the boundary layer separation from the surface and to make the laminar flow region encapsulate the airfoil surface, vortex generator (VG) was introduced on the blade [3]. Florian and Stillfried [17] found that vortex generator caused a disturbed turbulent flow leading to the reduced boundary layer separation than the normal body [4]. Vortex generators are aerodynamic devices with small vane like structures found in aerodynamic machines [5]. VG may be of rectangular or triangular in cross section, they should be also held at an angle to that of the wind flow, so that VGs do not affect the flow of air. Lin [8] had found that vortex generator created vortices near the flow separation which led to the reattachment of the flow over airfoil [6]. Vortex generators are controlled and act as flow regulators. NASA-McDonnell Douglas Aerospace tested VGs with various wind blades in the wind tunnel and found that the lift coefficient increased by 10% and drag coefficient by 40% [7]. Researchers working on vortex generators have found that the position of VGs should closer to the leading edge for symmetrical airfoils and for cambered airfoils, the position can be varied [8].

2. Effect of Bumped Leading Edge

Chen et al. [13] on the bumped leading edged airfoil stated that the disturbances caused to the fluid flow lead to the re-attachment of the boundary layer, which delayed the stalling and increased the performance of blade [9]. Hence, the wind turbine blades can be operated with high angle of attack, which in turn will increase the coefficient of lift. The VG modified blades will be most suitable for small wind turbines, which operate at low wind speeds.

Weitzman and Lambert [10] found that humpback whales were found using their flippers at higher operating angles before stall would occur, thereby reducing the boundary layer separation. The cross section of the whale flipper looks similar to that of an aircraft wing. This comparison led Fish et al. [6] to evaluate the potential to analysis the tubercles in air.

For large wind turbine blades operating at high wind speed stronger generators can be employed. But VGs were not so effective at low wind speeds. The lift coefficient can be increased by increasing the AOA. Eventually, increasing the AOA attack leads the flow to stall [11]. Stalling, caused due to high AOA and wind direction, is difficult to predict. This constrain limited the AOA to the minimum level. The efficiency of the wind turbine gets reduced due to the low AOA. Hence, for the wind turbines operating in low wind speed, to improve the operating efficiency, the normal blades can be replaced with whale flippers. Fish et al. [6] work on blades with whale flippers proved that for scalloped leading edge, the AOA can be increased upto 17° rather than the maximum of 12° for normal blades [12]. Gawad [1], in his study had found that, the AOA got increased upto 17° by incorporating the tubercles in a normal blade by 10% of the chord length to the leading edge of a NACA 0012 airfoil. The study by Čarija et al. [11] on the whale flipper leading edge showed a 50% increase in lift force between AOA of 0-20 [14].

3. Blade Design

A blade with NACA 0012 profile was designed for a 600 watts horizontal axis wind turbine with optimized parameters in order to avoid the major losses like blade profile loss, tip speed loss, solidity ratio, etc. One blade was created with smooth leading edge and the other blade was created with bumps on the leading edge keeping the smooth leading edged blade as reference.

3.1. Parameters optimization

Higher the number of blades better will be the overall power generation due to high interaction of surface with air motion, but more the number blades, the solidity ratio get increased, thereby reducing the airflow. Therefore, the optimum numbers of blades for commercial turbines are 3 only [15]. Applications like water pumping, milling, etc., require high initial torque for which the number of blades can be increased accordingly.

In this study, three bladed wind turbine used for power generation was considered. The tip speed ratio (TSR) was chosen such that the tip loss was minimum and vortices near the blade tip to be low, in order to improve the performance of the wind turbine. The TSR was chosen as 7 (design tip speed ratio (λ_d), as it gives maximum value of coefficient of performance (C_p) for three bladed turbines [17].

4. Modeling of Blade Geometry

The power extracted from the wind was calculated based on the kinetic energy of the wind equation (1):

$$P = \frac{1}{2} mv^2 = \rho A v^3 C_p, \tag{1}$$

$$C_p = \left(\frac{16}{27}\right)\lambda\left[\lambda + \frac{1.32 + \left(\frac{\lambda - 8}{20}\right)^2}{N^{2/3}}\right] - \frac{0.57\lambda^2}{\frac{C_L}{C_D}\left(\lambda + \frac{1}{2N}\right)}. \tag{2}$$

From equations (1) and (2), the swept area or the diameter of the wind turbine was computed as 2.2m,

$$\lambda_{rd} = \lambda \frac{r}{R}, \tag{3}$$

$$\phi = 0.667 \tan^{-1}\left(\frac{1}{\lambda_{rd}}\right), \tag{4}$$

$$C = \frac{8\pi r(1 - \cos\phi)}{\lambda_{rd}}. \tag{5}$$

The cord length at various sections of the blade from root to tip was computed using equations (3)-(5), and is tabulated in Table 1.

Table 1. Blade speed ratio and chord length

Blade segment	Radius (*r*) m	Speed ratio (λrd)	Chord length (c)
1	0.2	1.4	0.302
2	0.4	2.8	0.0993
3	0.6	4.2	0.043
4	0.8	5.6	0.024
5	1.0	7	0.016

4.1. Modeling of smooth edge blade

The coordinate points of NACA 0012 were retrieved from the UIUC airfoil coordinate database and into *X* and *Y* ordinates based on the chord length calculated for various sections. The model was drawn in ICEM by importing the coordinate points and tracing their respecting curves and lofting them.

4.2. Creation of bumped leading edge wing

The bumped model was generated by increasing and decreasing 10% of cord length alternately from the leading edge of the normal smooth blade. The wavelength of the sine wave shaped leading edge is equal to near every section of the blade. The area of cross section was maintained constant by alternative increase and decrease of the cord length along the leading edge of the blade profile.

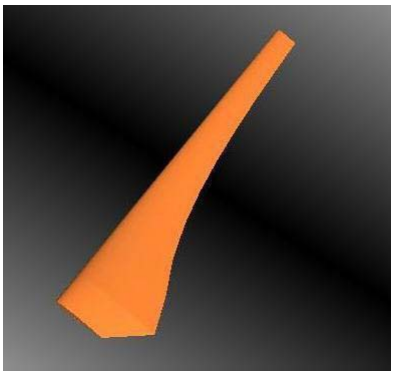

Figure 1. Smooth leading edge blade.

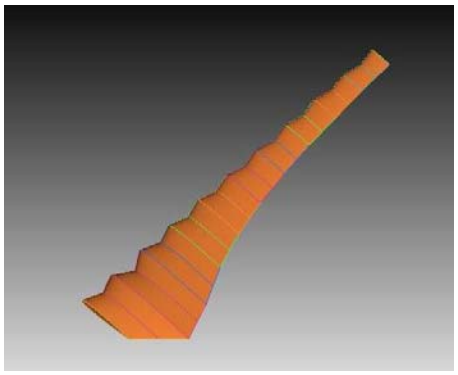

Figure 2. Bumped leading edge blade.

Figures 1 and 2 describe the profile shapes of both the smooth leading edge blade and modified bumped leading edge blade, respectively, which were created in the ICEM CFD for the purpose the computational analysis.

5. Computational Analysis Methodology

In order to reduce the computational load on the computer, a section of the blade with 3:1 reduced scale was considered for the analysis. This reduced the complexity of meshing and the number of nodes to be analyzed. The dimensions of the blade sections were tabulated in Table 2.

Table 2. Specifications of the blades

Parameters	Smoothed blade section	Bumped edge blade section
Chord length (L_C)	93.5mm	93.5mm
Blade length	100mm	100mm
Maximum bump (A)	-	9.35mm
Width of the bump (w)	-	$0.3L_C$ = 28mm

Figures 3(a) and 3(b) show the blade profile of both smooth and bumped blades, respectively, which are modeled using ICEM CFD and considered for the numerical analysis.

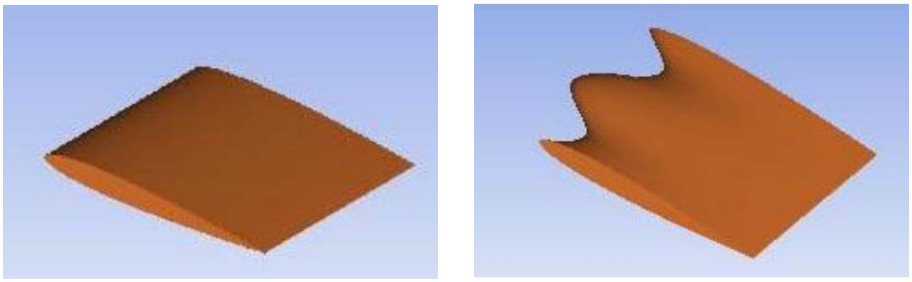

(a) Normal blade profile (b) Modified blade profile

Figure 3. Section of blade profiles.

6. Domain Creation and Meshing

The computational domain was created similar to an open atmospheric environment in which the wind turbine would operate. The domain was created as rectangular box with inlet as 7 times the chord length (L_C), outlet at 12 L_C from the trailing edge and 7 L_C on upper and lower sides.

The meshing was done using ICEM CFD with hexahedral discretization of the domain into elements. The total number of elements for both the blades was closely to 9 lakhs elements (Table 3). O-grid type mesh was used for meshing. The profile was meshed using line meshing options with 0.2mm mesh at the leading and the trailing edges. Very fine meshing at the vicinity of the blade surface ensures accurate capturing of the flow characteristics near the blade. As larger domain was modeled to capture the real time condition and in order to reduce the overall mesh count, the area away from the blade geometry was captured with coarse mesh (Figure 4).

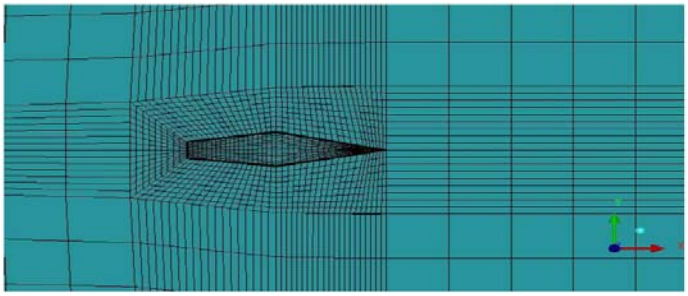

Figure 4. Mesh with O-grid around airfoil.

Table 3. Mesh properties

Mesh size	Normal blade	Modified blade
Elements	849408	885064
Nodes	818388	838143

7. Computational Setup

The computational analysis was done using the solver Fluent V6. Two equation models will be required to solve the model, if the flow involves laminar, turbulent, compressible, incompressible, steady and unsteady flows. The viscous *k-e* two equation model was considered for the study in this work. The boundary conditions at the inlet on the leading edge side were considered as velocity inlet $V_m = 15\text{m/s}$. The outlet boundary condition on the trailing edge side was considered as pressure outlet. The Reynolds number was 1×10^6 for the air velocities. The top and bottom sides over the top and lower surfaces of the blade were considered as no slip wall boundary condition. The encompassing domain surfaces were considered as no slip wall boundary condition. The fluid medium was air with an average temperature of 30°C. The pressure was computed automatically by the solver for the given conditions. The iterations were carried out for different angles of attack from 0° to 35° for the given velocity condition. The convergence limit was set at 1×10^{-5}. For each of the iterations, the pressure plot and the velocity plot were obtained. Coefficient of lift (C_L) and coefficient of drag (C_D) were plotted for different AOA to compare the performance of both the airfoils.

8. Results and Discussion

Wind turbine blades are the elements which convert the available kinetic energy in the wind into rotating mechanical energy. The aerodynamic shape of the blade produces two forces lift and drag, when the air flows over the blade. The lift and drag are the most important aerodynamic characters of any airfoil. In a wind turbine, the objective is to maximize the lift and

minimize the drag. After convergence, the lift and drag forces induced were evaluated based on coefficient of lift (C_L) and coefficient of drag (C_D), C_L and C_D were computed using equations (6) and (7) and were plotted against various AOA Figures 5 and 6. Write

$$C_L = \frac{Lift\ \ force}{\frac{1}{2}\rho A v^2}, \tag{6}$$

$$C_d = \frac{Drag\ \ force}{\frac{1}{2}\rho A v^2}. \tag{7}$$

The C_L versus AOA plot in Figure 5 describes the lift produced by the airfoil for the both the sections. For the smooth leading edged blade airfoil, the coefficient of lift produced between the most commonly used range of AOA of 7° to 12° was from 0.7 to 0.35, The C_L was 0.92 at 15°, which was maximum and there after remains constant or starts reducing. For the bumped leading edged blade airfoil, the coefficient of lift up to 10° of angle of attack was similar to that of smooth edged airfoil, but increase in AOA after 10° had produced increase in lift coefficient. The lift coefficient at 15 was 1, which was 8.7% higher than the smooth edged blade. The maximum C_L of 1.14 was produced at an angle of attack of 25°, whereas, for smooth edged airfoil, the flow got stalled above 15°. The overall maximum increase in the lift coefficient was 24% for the bumped leading edged airfoil section over the normal smooth edged blade airfoil.

From the plot coefficient of drag versus AOA Figure 6, the drag coefficient was more or less equal for both the airfoil sections. The drag was minimum at 0° angle of attack because of the symmetrical section of the airfoil. The drag coefficient was 0.4 for the angle of attack of 25°, for which maximum lift produced for the bumped leading edge airfoil.

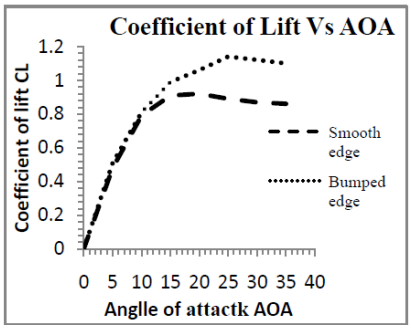

Figure 5. Coefficient of lift versus AOA.

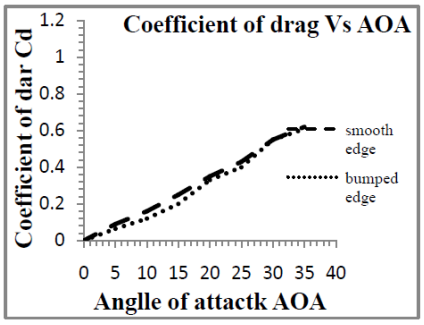

Figure 6. Coefficient of drag versus AOA.

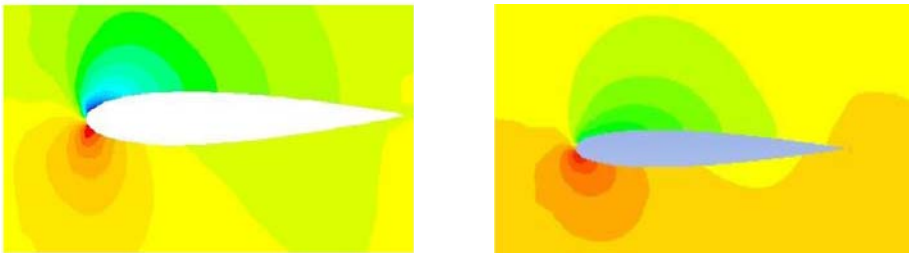

(a) Smooth edged blade profile (b) Bumped edge blade profile

Figure 7. Pressure plot for the airfoil sections.

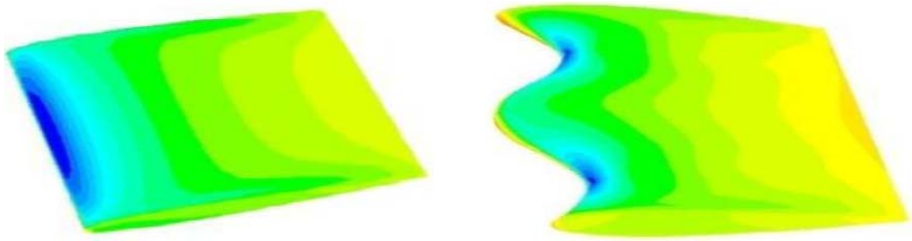

(a) Smooth edged blade (b) Bumped edge blade

Figure 8. Pressure intensities at the leading edge.

The pressure plot shown in Figures 7 and 8 describes the intensities of pressure over the airfoil section and at the leading edge of both the smooth edged and bumped edge blade airfoil sections. From Figure 7, it was observed that the intensity of pressure was very high at the leading edge for both the blade sections. For the smooth edged blade, the pressure was very

high on the lower surface and very close to the leading edge. On the upper surface, the pressure distribution varies in a very high order and within one third of chord distance, this shows that the boundary layer got detached and stall occurred at that area. The air which was flowing over the airfoil, flows well above the surface clearly indicating the detachment. On the bumped leading edge, the intensity of pressure was comparatively low at the leading and at the lower surface, the pressure distribution was comparatively uniform over both the surfaces. The pressure distribution on the top surface ranged from –1.48Pa to –0.362Pa gauge pressure and on the bottom surface, it was from +0.76Pa to +0.19Pa. It was evident from the above figures that the flow energy was converted into pressure energy on the impact of air on the leading edge. Since the intensity of pressure and the area impacted was more on the smooth edged blade section, the loss of flow energy was more comparative to the bumped edged blade section. This loss of energy had resulted in reduced lift coefficient for the smooth edged blade section, whereas the bumped edged blade section had more uniform flow over the blade section encapsulating the blade, the loss of energy due to the impact of air on the leading is low, as the bumped portions guide the air motion to the voids, the area impacted was very small, due to which the maximum of the flow energy was converted into the lift force.

9. Conclusion

The wind turbines operating in low wind speed required a very high lift coefficient. One way of increasing the lift coefficient was by increasing the angle of attack, but, when the AOA was increased beyond a certain limit, stall occurs detaching the boundary layer, which is not a desired effect. Therefore, the optimum AOA for the commercial wind turbines available so far, with smooth edged leading edge ranges between 5° to 12°. From the above numerical analysis, it was found by modifying the blade profiles, with bumped leading edges, the AOA can be increased to as high as 25°. The increase in the AOA resulted in increased lift coefficient of 24%. The bumped leading edge profile can be well employed for the wind turbines operating at low wind regime and urban environment.

References

[1] Ahmed Farouk Abdel Gawad, Utilization of whale-inspired tubercles as a control technique to improve airfoil performance, Transaction on Control and Mechanical Systems 2(5) (2013), 212-218.

[2] Alessandro Corsini, Giovanni Delibra and Anthony G. Sheard, On the role of leading-edge bumps in the control of stall onset in axial fan blades, Journal of Fluids Engineering 135(8) (2013), 081104-1.

[3] A. Dropkin, D. Custodio, C. W. Henoch and H. Johari, Computation of flow field around an airfoil with leading-edge protuberances, Journal of Aircraft 49(5) (2012), 1345-1355.

[4] D. Custodio, C. W. Henoch and H. Johari, Aerodynamic characteristics of finite span wings with leading-edge protuberances, AIAA Journal 53(7) (2015), 1878-1893.

[5] D. S. Miklosovic, M. M. Murray, L. E. Howle and F. E. Fish, Leading-edge tubercles delay stall on humpback whale (*Megaptera novaeangliae*) flippers, Phys. Fluids 16(5) (2004), L39-L42.

[6] F. E. Fish, P. W. Weber, M. M. Murray and L. E. Howle, The tubercles on humpback whales' flippers: application of bio-inspired technology, Integrative and Comparative Biology 51(1) (2011), 203-213.

[7] F. E. Fish and Juliann M. Battle, Hydrodynamic design of the humpback whale flipper, Journal of Morphology 225 (1) (1995), 51-60.

[8] John C. Lin, Review of research on low-profile vortex generators to control boundary-layer separation, Progress in Aerospace Sciences 38(4) (2002), 389-420.

[9] M. Asli, B. M. Gholamali and A. M. Tousi, Numerical analysis of wind turbine airfoil aerodynamic performance with leading edge bump, Math. Probl. Eng. 2015 (2015), Article ID 493253, 8 pp.

[10] Sam Weitzman and Ann Lambert, More efficient helicopter blades based on whale tubercles, J. Emerging Investigators 2 (2013), 66-72.

[11] Z. Čarija, E. Marušić, Z. Novakm and S. Fućak, Numerical analysis of aerodynamic characteristics of a bumped leading edge turbine blade, Engineering Review 34(2) (2014), 93-101.

[12] J. D. Anderson, Fundamentals of Aerodynamics, McGraw-Hill, 2007.

[13] J. H. Chen, S. S. Li and V. T. Nguyen, The effect of leading edge protuberances on the performance of small aspect ratio foils, International Symposium on Flow Visualization, 2012.

[14] Paul W. Weber, Laurens E. Howle and Mark M. Murray, Lift, drag, and cavitation onset on rudders with leading-edge tubercles, Marine Technology 47(1) (2010), 27-36.

[15] Hugo T. C. Pedro and Marcelo H. Kobayashi, Numerical study of stall delay on humpback whale flippers, 46th AIAA Aerospace Sciences Meeting and Exhibit, 2008.

[16] N. Karthikeyan and S. Sudhakar, Experimental studies on the effect of leading edge tubercles on laminar separation bubble, AIAA SciTech, 2014.

[17] M. Florian and V. Stillfried, Computational studies of passive vortex generators for flow control, Stockholm: KTH, 2009, 108 pp.